

4.4 Regional Spectral Model (JMA-RSM0404)

4.4.1 Introduction

The model is a spectral limited area model which has 40 σ -p hybrid vertical levels and horizontal resolution of 20 km. RSM produces 51-hour forecasts twice a day with the lateral boundary condition supplied by the Global Spectral Model (GSM) every three hours. The major objectives of RSM are: (1) to predict meso- α and - β scale phenomena over and around Japan, especially those which are strongly controlled by the orography, (2) to supply quantitative forecast of surface temperature, wind and precipitation amount, (3) to provide information for local aviation uses, (4) to provide the lateral boundary condition for the Meso Scale Model(MSM).

4.4.2 Structure of the model

(a) Vertical levels

A σ -p hybrid coordinate is introduced in the vertical. The definition of half-level pressure is described in equation (4.2.9) and full-level pressure is expressed by $p_k = \exp((p_{k-1/2} \ln(p_{k-1/2}) - p_{k+1/2} \ln(p_{k+1/2})) / \Delta p_k - 1)$ except for the top level kmax. The top full-level pressure is $\Delta p_{k\text{max}-1/2}/2$. The RSM has 40 vertical levels as shown in Table 4.4.1. The vertical resolution is higher in the lower atmosphere for better simulation of the planetary boundary layer processes.

Table 4.4.1 Vertical levels of RSM.

level (k)	p_k (hPa)	Δp_k (hPa)	$A_{k-1/2}$ (hPa)	$B_{k-1/2}$
40	10	20	20.	0.000
39	30	20	40.	0.000
38	52	25	65.	0.000
37	78	25	85.	0.005
36	102	25	99.	0.016
35	127	25	109.	0.031
34	152	25	116.	0.049
33	177	25	121.	0.069
32	202	25	124.	0.091
31	227	25	126.	0.114
30	252	25	126.	0.139
29	277	25	126.	0.164
28	302	25	124.	0.191
27	330	30	121.	0.224
26	360	30	117.	0.258
25	390	30	113.	0.292
24	420	35	107.	0.328
23	452	35	100.	0.370
22	487	35	92.	0.413
21	522	35	84.	0.456

level (k)	p_k (hPa)	Δp_k (hPa)	$A_{k-1/2}$ (hPa)	$B_{k-1/2}$
20	557	35	75.	0.500
19	592	35	66.	0.544
18	627	35	56.	0.588
17	662	35	47.	0.633
16	697	35	38.	0.677
15	732	35	29.	0.721
14	765	30	22.	0.758
13	795	30	15.	0.795
12	825	30	10.	0.830
11	852	25	6.	0.859
10	877	25	3.	0.887
9	900	20	1.	0.909
8	920	20	0.	0.930
7	937	15	0.	0.945
6	953	15	0.	0.960
5	965	10	0.	0.970
4	975	10	0.	0.980
3	985	10	0.	0.990
2	992	5	0.	0.995
1	997	5	0.	1.000

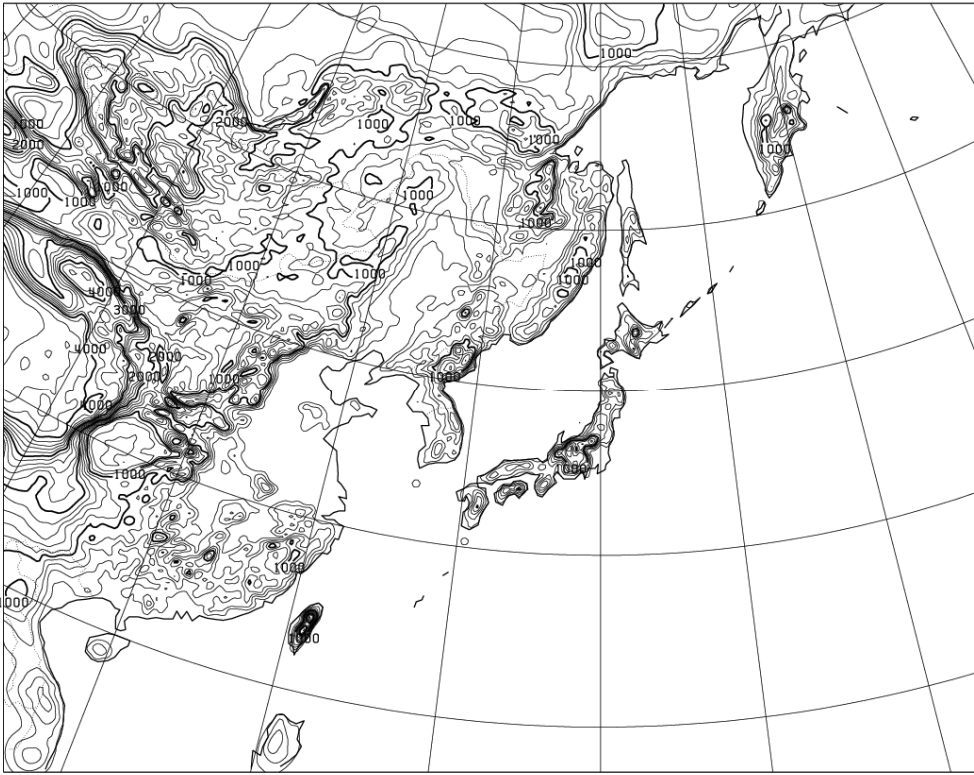


Fig. 4.4.1 Forecast domain and topography of RSM. Contour interval is 200m.
Original data of topography is GTOPO30.

(b) Forecast area and transform grid

Fig. 4.4.1 shows the forecast domain and topography of RSM. An envelope orography is used. The model has a regular square transform grid of 325×257 with a grid distance of 20km at 30° and 60° N on a Lambert projection plane. RSM adopts a circular wave truncation at 214 and 169 in the x and y direction, respectively (see section 4.4.4).

4.4.3 Basic equations

The model is formulated in terms of the primitive equations for momentum, mass, specific humidity, and virtual temperature using advection forms. They are expressed as follows.

Equations of motion

$$\begin{aligned} \frac{\partial u^*}{\partial t} = & -m^2 \left(u^* \frac{\partial u^*}{\partial x} + v^* \frac{\partial u^*}{\partial y} \right) - \frac{1}{2} u^* \left(u^* \frac{\partial m^2}{\partial x} + v^* \frac{\partial m^2}{\partial y} \right) - \dot{\eta} \frac{\partial u^*}{\partial \eta} \\ & - \left(\frac{\partial \phi}{\partial x} + R_d T_v \frac{\partial \pi^*}{\partial x} \right) + v^* \left\{ f + \frac{1}{2} \left(u^* \frac{\partial m^2}{\partial y} - v^* \frac{\partial m^2}{\partial x} \right) \right\} + D_u - \frac{1}{m\rho} \frac{\partial \tau_x}{\partial z} \end{aligned} \quad (4.4.1)$$

$$\begin{aligned} \frac{\partial v^*}{\partial t} = & -m^2 \left(u^* \frac{\partial v^*}{\partial x} + v^* \frac{\partial v^*}{\partial y} \right) - \frac{1}{2} v^* \left(u^* \frac{\partial m^2}{\partial x} + v^* \frac{\partial m^2}{\partial y} \right) - \dot{\eta} \frac{\partial v^*}{\partial \eta} \\ & - \left(\frac{\partial \phi}{\partial y} + R_d T_v \frac{\partial \pi^*}{\partial y} \right) - u^* \left\{ f + \frac{1}{2} \left(u^* \frac{\partial m^2}{\partial y} - v^* \frac{\partial m^2}{\partial x} \right) \right\} + D_v - \frac{1}{m\rho} \frac{\partial \tau_y}{\partial z} \end{aligned} \quad (4.4.2)$$

Thermodynamic equation

$$\frac{\partial T_v}{\partial t} = -m^2 \left(u^* \frac{\partial T_v}{\partial x} + v^* \frac{\partial T_v}{\partial y} \right) - \dot{\eta} \frac{\partial T_v}{\partial \eta} + \frac{R_d T_v}{c_p p} \frac{dp}{dt} + \frac{Q^*}{c_p} + \frac{1}{c_p \rho} \frac{\partial F_H}{\partial z} + D_T \quad (4.4.3)$$

Equation of water vapor

$$\frac{\partial q}{\partial t} = -m^2 \left(u^* \frac{\partial q}{\partial x} + v^* \frac{\partial q}{\partial y} \right) - \dot{\eta} \frac{\partial q}{\partial \eta} + M + \frac{1}{\rho} \frac{\partial F_q}{\partial z} + D_q \quad (4.4.4)$$

Tendency equation and continuity equation

$$\frac{\partial \pi^*}{\partial t} = -\frac{m}{p_s} \int_0^1 \nabla \left(\frac{\partial p}{\partial \eta} \mathbf{v}^* \right) d\eta \quad (4.4.5)$$

$$\dot{\eta} \frac{\partial p}{\partial \eta} = -\frac{\partial p}{\partial t} - m^2 \int_0^\eta \nabla \left(\frac{\partial p}{\partial \eta} \mathbf{v}^* \right) d\eta \quad (4.4.6)$$

Hydrostatic equation

$$\frac{\partial \phi}{\partial \eta} = -R_d T_v \frac{\partial \ln p}{\partial \eta} \quad (4.4.7)$$

where $\mathbf{v}^* = (u^*, v^*) = (u/m, v/m)$ and (u, v) are (x, y) component of wind vector, m is map factor, ϕ is geo-potential height, R_d is gas constant of dry air, T_v is virtual temperature, q is specific humidity of water vapor (kg/kg), p is pressure, p_s is surface pressure and $\pi^* = \ln(p_s)$, ρ is density of dry air, f is Coriolis parameter, (D_u, D_v, D_T, D_q) are horizontal diffusion for u and v component of wind, virtual temperature and water vapor, (τ_x, τ_y) are shear stress, $c_p = c_{pd} + (c_{pv} - c_{pd}) q$ and (c_{pd}, c_{pv}) are specific heat of (dry air, water vapor) at constant pressure, (F_H, F_q) are vertical eddy flux heat and moisture, (Q^*, M) are heat and moisture source/sink per unit mass, respectively.

4.4.4 Spectral representation

The spectral method for a time dependent lateral boundary condition described in Tatsumi (1986) (TA86, hereafter) is adopted for this model. For physical space variables, we introduce a column matrix $\underline{\mathbf{a}}$ with $4N+1$ elements (N being the number of the model vertical levels).

$$\underline{\mathbf{a}} = \left(u^*_{k=1}, \dots, u^*_{k=N}, \dots, v^*_{k=N}, \dots, T_v^*_{k=N}, \dots, q^*_{k=N}, \pi^* \right)^T \quad (4.4.8)$$

If a field satisfies the rigid boundary condition, the field can be expanded in double Fourier series as shown in eqs. (4.4.9) and (4.4.10). However, the real atmosphere does not satisfy the rigid boundary condition at the lateral boundaries in general. In Tatsumi's regional spectral method, the large scale fields $\underline{\mathbf{a}}_N$ which satisfy the time-dependent lateral boundary conditions are subtracted from the actual fields $\underline{\mathbf{a}}$ so that the remaining fields satisfy the rigid boundary conditions and can be expanded in the double Fourier series;

$$\underline{\mathbf{a}} - \underline{\mathbf{a}}_N = \underline{\mathbf{a}}_0 = \sum_m \sum_n \underline{A}_{mn}^0(t) F^0(m\hat{x}, n\hat{y}) \quad (4.4.9)$$

where \underline{A}_{mn}^0 is an orthogonal wave component and F^0 is an orthogonal double Fourier function defined as

$$F^0(m\hat{x}, n\hat{y}) = \begin{pmatrix} \sin(m\hat{x})\cos(n\hat{y}) \\ \cos(m\hat{x})\sin(n\hat{y}) \\ \cos(m\hat{x})\cos(n\hat{y}) \\ \sin(m\hat{x})\sin(n\hat{y}) \end{pmatrix} \quad \text{for} \quad \begin{pmatrix} u^* \\ v^* \\ T_v, \pi^* \\ q \end{pmatrix} \quad (4.4.10)$$

where \hat{x} and \hat{y} are horizontal coordinates normalized by the sizes of the forecast domain L_x and L_y ;

$$\hat{x} = \frac{\pi x}{L_x}, \hat{y} = \frac{\pi y}{L_y} \quad (0 \leq \hat{x}, \hat{y} \leq \pi)$$

There is arbitrariness in the selection of $\underline{\mathbf{a}}_N$, and TA86 chooses a combination of sine and cosine functions (F^N) .

$$\underline{\mathbf{a}}_N = \sum_m \sum_n \underline{A}_{mn}^N F^N(m\hat{x}, n\hat{y}) \quad (4.4.11)$$

The large scale fields $\underline{\mathbf{a}}_N$ or non-orthogonal wave components \underline{A}_{mn}^N prescribed to satisfy the lateral boundary conditions using the values or derivatives of the outer model at the boundary.

Then the final form of the spectral representation becomes

$$\underline{\mathbf{a}} = \sum_m \sum_n \underline{A}_{mn}(t) F^*(m\hat{x}, n\hat{y}) \quad (4.4.12)$$

$$\underline{A}_{mn}(t) = \underline{A}_{mn}^0(t) + \underline{A}_{mn}^N \quad (4.4.13)$$

where \underline{A}_{mn} is a wave component for physical space and F^* a modified double Fourier series defined as follows:

$$F^*(m\hat{x}, n\hat{y}) = \begin{pmatrix} \sin^*(m\hat{x}) \cos^*(n\hat{y}) \\ \cos^*(m\hat{x}) \sin^*(n\hat{y}) \\ \cos^*(m\hat{x}) \cos^*(n\hat{y}) \\ \sin^*(m\hat{x}) \sin^*(n\hat{y}) \end{pmatrix} \quad \text{for} \quad \begin{pmatrix} u^* \\ v^* \\ T_v, \pi^* \\ q \end{pmatrix} \quad (4.4.14)$$

where

$$\begin{aligned} \sin^*(m\hat{x}) &= \begin{cases} \sin(m\hat{x}) & \text{for } m = 1, 2, 3, \dots \\ \cos(-m\hat{x}) & \text{for } m = 0, -1 \end{cases} \\ \cos^*(m\hat{x}) &= \begin{cases} \cos(m\hat{x}) & \text{for } m = 0, 1, 2, \dots \\ \sin(-m\hat{x}) & \text{for } m = -1, -2 \end{cases} \end{aligned} \quad (4.4.15)$$

and the summation over m and n in equation (4.4.12) are taken followed by the definition of \cos^* and \sin^* .

An additional (or non-orthogonal) term \underline{A}_{mn}^N is prescribed from the outer model and only the \underline{A}_{mn}^0 components are prognostic. The prognostic equation for \underline{A}_{mn}^0 can be written in the following form.

$$\frac{\partial \underline{A}_{mn}^0}{\partial t} = \varepsilon_m \varepsilon_n \int \int_0^\pi F^0(m\hat{x}, m\hat{y}) \left\{ \frac{\partial \underline{\mathbf{a}}(t)}{\partial t} - \sum_k \sum_l \frac{\partial \underline{A}_{kl}^N}{\partial t} F^*(k\hat{x}, l\hat{y}) \right\} d\hat{x} d\hat{y} \quad (4.4.16)$$

where ε is a normalizing factor defined as

$$\varepsilon_m = \begin{cases} 1/\pi & \text{for } m = 0 \\ 2/\pi & \text{for } m = 1, 2, 3, \dots \end{cases}$$

The matrix $\partial \underline{\mathbf{a}}(t)/\partial t$ denotes the time tendency of all prognostic variables in physical space described in eqs. (4.4.1) - (4.4.5).

The elliptic wave truncation is adopted with a maximum wave number K_{\max} ($=214$);

$$\sqrt{m^2 + n^2} \leq K_{\max} \quad (4.4.17)$$

4.4.5 Vertical differencing scheme and time integration scheme

The vertical differencing scheme of the model is identical to that of Global Spectral Model (GSM) described in 4.2.2. A semi-implicit time integration scheme for the spectral limited area model described in TA86 is used for saving computational time. This is applied to linearized gravity wave terms in the divergence, virtual temperature and continuity equation. The time integration is made with the use of the leap-frog scheme with a time filter (Asselin, 1972).

4.4.6 Boundary relaxation

In order to reduce the spurious noise near the lateral boundary, the following boundary relaxation technique proposed by Davies (1976) is used.

$$\frac{\partial \underline{A}_{mn}^0}{\partial t} = -\varepsilon_m \varepsilon_n \int_0^\pi F^0(m\hat{x}, n\hat{y}) \beta_0 (\underline{a} - \hat{\underline{a}}) d\hat{x} d\hat{y} \quad (4.4.18)$$

where \underline{a} and $\hat{\underline{a}}$ are inner and outer model grid point values, respectively. β_0 is chosen as

$$\beta_0 = \begin{cases} 1/2\beta_0^*(1 + \cos(l_b\pi/L_b)) & (0 \leq l_b \leq L_b) \\ 0 & (L_b \leq l_b) \end{cases}$$

and

$$1/\beta_0^* = 2/3 \text{ hours}$$

where L_b (=35) is the width of the relaxation area and l_b is the distance from the nearest boundary measured by the number of grid.

The lateral boundary conditions are constructed by linear interpolation with 3-hourly forecasts of GSM (see 4.2).

4.4.7 Horizontal diffusion

The forms of horizontal diffusion used in the model are

$$\begin{aligned} D_u &= -K_d \nabla^4 u^* \\ D_v &= -K_d \nabla^4 v^* \\ D_r &= -K_d \nabla^4 \left\{ T_v - \overline{p_s} \frac{\partial \overline{T}_v}{\partial p} \left(\frac{\partial p}{\partial p_s} \right)_n \pi^* \right\} \\ D_q &= -K_d \nabla^4 q \end{aligned} \quad (4.4.19)$$

where overbar means average on a model-level surface. The second term in the temperature diffusion is the correction for the height difference of model-level surface to reduce spurious vertical mixing along a steep mountain slope. The diffusion coefficient K_d is given by

$$K_a = \frac{1}{\tau_e} \left\{ \frac{(IM-1)d}{\pi K_{\max}} \right\}^4 \quad (4.4.20)$$

where τ_e ($= 12$ min.) is an e-folding time of the wave component of the shortest wave length in the model (wave number $K_{\max} = 214$), IM ($= 325$) is the transform grid number of x-direction, d is the grid distance of the model, respectively.

4.4.8 Physical process

(a) Surface fluxes

Surface fluxes are calculated with the following formula:

$$\begin{aligned} \tau_x / \rho &= C_m |\mathbf{V}_a| u_a \\ \tau_y / \rho &= C_m |\mathbf{V}_a| v_a \\ H &= -\rho c_p C_h |\mathbf{V}_a| (\theta_{va} - \theta_{vs}) \\ LE &= -L \rho C_h |\mathbf{V}_a| (q_a - q_s) \end{aligned} \quad (4.4.21)$$

and

$$\begin{aligned} |\mathbf{V}_a| &= \sqrt{u_a^2 + v_a^2} \\ q_s &= (1 - \beta) q_a + \beta q_{sat}(T_s) \end{aligned}$$

where T is temperature, θ_v is virtual potential temperature, H and LE are the sensible heat and latent heat flux, L is latent heat of vaporization, $q_{sat}(T)$ is saturation specific humidity at temperature T , and the subscripts a and s denote the values at the first vertical level and the earth's surface, respectively. β indicates evapotranspiration efficiency and is set constant during the time integration. For bulk coefficients of C_m and C_h , the formula proposed by Louis et al. (1980) is used and the difference of roughness parameters for the momentum and heat (or moisture) is taken into account.

$$\begin{aligned} C_m &= \left\{ \frac{k}{\ln(z_a/z_{0m})} \right\}^2 f_m(R_i, z_a/z_{0m}) \\ C_h &= \frac{k}{\ln(z_a/z_{0m})} \frac{k}{\ln(z_a/z_{0h})} f_h(R_i, z_a/z_{0m}, z_a/z_{0h}) \end{aligned} \quad (4.4.22)$$

where k is the von Karman's constant ($= 0.4$), z_0 is the roughness parameter, and R_i is the Richardson number given by

$$R_i = \frac{g z_a \Delta \theta_v}{\theta_{va} |V_a|^2} \quad (4.4.23)$$

$$\Delta \theta = \theta_a - \theta_s$$

$$\Delta \theta_v = \Delta \theta + 0.608 \theta_a \Delta q$$

where g is the gravity constant. The analytical expressions of the similarity functions in eq. (4.4.22) for the unstable case ($R_i < 0$) are

$$f_m = 1 - \frac{2bR_i}{1 + 3bc \left\{ \frac{k}{\ln(z_a / z_{0m})} \right\}^2 \sqrt{-\frac{R_i z_a}{z_{0m}}}} \quad (4.4.24)$$

$$f_h = 1 - \frac{3bR_i}{1 + 3bc \frac{k}{\ln(z_a / z_{0m})} \frac{k}{\ln(z_a / z_{0h})} \sqrt{-\frac{R_i z_a}{z_{0h}}}} \quad (4.4.25)$$

where $b = c = 5$.

For the stable case ($R_i > 0$)

$$f_m = \frac{1}{1 + 2bR_i / \sqrt{1 + dR_i}} \quad (4.4.26)$$

$$f_h = \frac{1}{1 + 3bR_i \sqrt{1 + dR_i}}$$

is used with $d = 5$. Roughness parameter z_{0m} for momentum and z_{0h} for heat and moisture are described in (d).

(b) Ground temperature

A four-layer model for the ground is used. The prognostic equations take the following form

$$\begin{aligned} \frac{\partial T_0}{\partial t} &= \frac{G_0}{\rho_g C_g \Delta Z_0} + \frac{2v_g}{\Delta Z_0 (\Delta Z_1 + \Delta Z_0)} (T_1 - T_0) \\ \frac{\partial T_1}{\partial t} &= -\frac{2v_g}{\Delta Z_1 (\Delta Z_1 + \Delta Z_0)} (T_1 - T_0) + \frac{2v_g}{\Delta Z_1 (\Delta Z_2 + \Delta Z_1)} (T_2 - T_1) \\ \frac{\partial T_2}{\partial t} &= -\frac{2v_g}{\Delta Z_2 (\Delta Z_2 + \Delta Z_1)} (T_2 - T_1) + \frac{2v_g}{\Delta Z_2 (\Delta Z_3 + \Delta Z_2)} (T_3 - T_2) \end{aligned} \quad (4.4.27)$$

where the subscript 0 denotes the surface layer, 1-3 denotes the vertical level of the underground. The T_3 is constant during the forecast. G_0 represents the heat flux into the ground and is derived from the sum of radiation (R_{net}), sensible heat (H) and latent heat flux (LE):

$$G_0 = R_{net} + H + LE. \quad (4.4.28)$$

The sensible heat and latent heat fluxes are calculated in the surface boundary layer scheme (eq. (4.4.21)). To take account of the diurnal variation of stomatal evapotranspiration activity, the equation for latent heat flux is written as follows:

$$\begin{aligned} LE &= -L \frac{1}{r} (q_a - q_s) \\ r &= r_s + \frac{1}{\rho C_h |\mathbf{V}_a|}, \quad r_s = \frac{r_n}{1 + F_{DSW}} + r_d \end{aligned} \quad (4.4.29)$$

where r_n and r_d are constant and the value of r_d is changed semi-annually for the warm and the cold season. R_{net} and F_{DSW} (downward short wave radiation at the ground surface) is calculated in the radiation process.

The surface temperature T_0 is used for calculating the radiation and heat fluxes at the ground surface. Climatological data described in (d.5) gives the initial ground temperature.

The heat capacity of the ground per unit volume ($\rho_g C_g$) and the heat diffusion coefficient (v_g) are taken to be

$$\rho_g C_g = 2.3 \times 10^6 \text{ J/m}^3 \text{ K}, \quad v_g = 7.0 \times 10^{-7} \text{ m}^2/\text{sec}$$

over the land,

$$\rho_g C_g = 8.4 \times 10^7 \text{ J/m}^3 \text{ K}, \quad v_g = 4.0 \times 10^{-7} \text{ m}^2/\text{sec}$$

over the snow covered area, and

$$\rho_g C_g = 1.9 \times 10^6 \text{ J/m}^3 \text{ K}, \quad v_g = 1.3 \times 10^{-6} \text{ m}^2/\text{sec}$$

over the ice covered area. The distribution of snow and ice is given as described in (d.3).

The trapezoidal implicit scheme is used for the time integration of the ground temperatures.

(c) Vertical diffusion above the surface layer

The level 2 version of the turbulent closure model proposed by Mellor and Yamada (1974) is used for vertical diffusions. The equations of the vertical diffusions are written using the z-coordinate as follows:

$$\begin{aligned}
\frac{\partial u}{\partial t} &= \frac{1}{\rho} (\rho K_m \frac{\partial u}{\partial z}) = \frac{1}{\rho} \frac{\partial \tau_x}{\partial z} \\
\frac{\partial v}{\partial t} &= \frac{1}{\rho} (\rho K_m \frac{\partial v}{\partial z}) = \frac{1}{\rho} \frac{\partial \tau_y}{\partial z} \\
\frac{\partial \theta_v}{\partial t} &= \frac{1}{\rho} (\rho K_h \frac{\partial \theta_v}{\partial z}) = \frac{1}{\rho C_p} \left(\frac{p_0}{p} \right)^\kappa \frac{\partial F_H}{\partial z} \\
\frac{\partial q}{\partial t} &= \frac{1}{\rho} (\rho K_h \frac{\partial q}{\partial z}) = -\frac{1}{\rho} \frac{\partial F_q}{\partial z} \\
K_m &= K_0 + l^2 \left| \frac{\partial V}{\partial z} \right| S_m \\
K_h &= K_0 + l^2 \left| \frac{\partial V}{\partial z} \right| S_h \\
(K_0 &= 1.0 m^2/s)
\end{aligned} \tag{4.4.30}$$

where S_m and S_h are functions of flux Richardson number (Mellor and Yamada (1974)).

The length scale l is given by

$$l = \frac{kz}{1 + kz/l_0}, \quad l_0 = 100(m)$$

where k is von Karman's constant.

The non-local PBL scheme proposed by Tohen and Mahrt(1986) is adopted for the area of strong unstable in low levels. The above vertical diffusion process is applied through the whole model layers. An over-implicit time integration scheme is used for these terms to prevent numerical instability.

(d) Surface data

(d.1) Roughness parameter

(d.1.1) Over land

Different values of the roughness parameter are used for the warm and cold seasons. They are determined from the vegetation and land use datasets produced by the Ministry of Land, Infrastructure and Transport for the Japan area and by NASA (Matthews, 1983) for the other area. A constant value of 10cm is set as a roughness parameter for heat and moisture .

(d.1.2) Over the sea

To incorporate the dependency of roughness parameter on wind speed over the sea, we use the following relation described by NPD/JMA (1986).

$$z_0 = -34.7 \times 10^{-6} + 8.28 \times 10^{-4} u^* \quad \text{for } u_{10} \leq 25 \text{m/s}$$

$$z_0 = -0.227 \times 10^{-2} + 3.39 \times 10^{-3} u^* \quad \text{for } u_{10} \geq 25 \text{m/s}$$

where u^* is a friction velocity and u_{10} is a wind speed at 10m height above sea level. The minimum value of the roughness parameter is set at 1.5×10^{-5} m. The above expression is derived from Kondo (1975).

The same roughness parameter is used for momentum and heat. However, the difference of roughness parameters is considered in the calculation of surface fluxes. The last two equations in (4.4.21) are replaced by

$$\theta_{va} - \theta_{vs} = \theta^* \left(\frac{u^*}{C_h |V_a|} + B_h^{-1} \right)$$

$$q_a - q_{sat}(T_s) = q^* \left(\frac{u^*}{C_h |V_a|} + B_e^{-1} \right)$$

as described by Kondo (1975). For the correction factor B_h^{-1} B_e^{-1} over sea, Kondo (1975) proposed the following formulae based on the various observations:

$$B_e^{-1} = \frac{1}{k} \ln \left(\frac{\nu + k u^* z_0}{\alpha} \right)$$

$$B_h^{-1} = \frac{1}{k} \ln \left(\frac{\nu + k u^* z_0}{D} \right)$$

where α is the thermodynamic conductivity of air, ν is the kinetic viscosity of air, and D is the molecular diffusion coefficient of air.

(d.2) Evapotranspiration efficiency

The evapotranspiration efficiency for the warm and the cold season are obtained from the same datasets as the roughness parameter. Over a snow- or ice-covered area, the value is set as 1.0.

(d.3) Snow and sea ice

Snow or ice covered areas are treated as land for surface processes of the model. The analyzed snow cover data are used over Japan, and global snow depth analysis data described in subsection 3.9 are used over the other area. The ice cover is based on sea ice analysis conducted by JMA.

(d.4) Surface albedo

Surface albedo for each season are obtained from the same datasets as the roughness parameter. Over snow or ice covered area, the value is set to 0.6.

(d.5) Climatological ground temperature

Climatological data for the ground temperature are obtained in the following way. First, the monthly mean temperatures of standard pressure levels is calculated from the objective analysis during 1985 and 1986. Next, these data are interpolated vertically to the model ground surface. Then, only the annual mean and the first harmonic component of the surface temperature are extracted to obtain the climatological underground temperature of the i-th ground layer with the following equation.

$$T_i = \hat{T} + A \exp(-z_i / d) \cos\{2\pi/365 \times (D - P) - z_i / d\}$$

where \hat{T} is the mean soil temperature, A and P are the amplitude and the phase of the annual component of the surface temperature, respectively, z_i is the depth of the i-th ground layer and d (=2.65m) is the e-folding depth and D is the number of day from the beginning of the year.

(e) Parameterizations of precipitation

The prediction of precipitation contains four processes; large scale condensation, middle level convection, cumulus convection with its roots in the PBL and evaporation of raindrops.

(e.1) Large scale condensation

Condensation occurs when the predicted specific humidity (q) exceeds the saturated value at the predicted temperature T. The adjusted values of specific humidity (q') and temperature (T') are given by

$$\begin{aligned} q' &= q - \frac{q - q_{sat}(T)}{1 + \frac{L^2}{C_p} \frac{\varepsilon q_{sat}(T)}{RT^2}} \\ T' &= T + \frac{L}{C_p} (q - q') \end{aligned} \quad (4.4.31)$$

where $\varepsilon = 0.622$.

(e.2) Mid-level convection

The moist convective adjustment scheme proposed by Benwell and Bushby (1970) and Gadd and Keers (1970) are applied to unstable mid-levels. When the temperature lapse rate exceeds the critical value Γ_c , the temperature and the specific humidity are adjusted so that the lapse rate is equal to the critical value Γ_c . Γ_c is a function of relative humidity (Rh) and is given by

$$\Gamma_c = \frac{1}{1 - Rh_c} \{ \Gamma_d (1 - Rh) + \Gamma_m (Rh - Rh_c) \} \quad (4.4.32)$$

where Rh_c ($=0.5$) is a critical relative humidity. The lapse rate is not adjusted when Rh is smaller than Rh_c . This process is applied to the vertical levels above the cloud base of the cumulus convection with its roots in the PBL.

(e.3) Cumulus convection with its roots in the PBL

An economical version of the Arakawa - Schubert scheme (1974), which is implemented in GSM is also implemented in RSM, though there are several differences between them. Refer subsection 4.2.4 with the following exceptions;

- (1) the cloud base level is fixed near 950hPa.
- (2) the effect of turbulence on the moist static energy at the cloud base is not considered.
- (3) the range of λ is set between $2 \times 10^{-5} \text{ m}^{-1}$ and $4 \times 10^{-3} \text{ m}^{-1}$. The lower limit of the entrainment rate is that proposed by Tokioka et al. (1988).
- (4) as for the evaporation at the cloud top, all the remains of condensed water is converted into rain water.
- (5) the effect of wind shear is not considered in the re-evaporation.
- (6) Instead of equation (4.2.31), the following equation is used for the upward mass flux,

$$\frac{dM_B}{dt} = \frac{A(\lambda) - A_0(\lambda)}{2\alpha(\lambda)}$$

- (7) the downdraft is initiated at the level of the minimum moist energy.
- (8) the downdraft mass flux M_d at the cloud base is specified so that the re-evaporation of rainwater moistens the cloud base to its saturation.
- (9) Mid-level convection for RSM is described in 4.4.8(e-2).
- (10) convective momentum transport described in 4.2.4(e) is not adopted.

(e.4) Evaporation of raindrops

Condensed raindrops may evaporate while they fall down to the ground. In order to compute evaporation the rate of the raindrops ($P7$, unit: g/(g s)), The following formula proposed by Ogura and Takahashi (1971) is adopted:

$$P7 = -\frac{C}{\rho} \frac{(Q_v / Q_{vs} - 1)(\rho Q_r)^{0.525}}{5.4 \times 10^{-5} + 0.41 \times 10^7 / e_{vs}}$$

$$C = 1.6 + 0.76 \times 10^{-3} (V_r)^{1.5} \quad (4.4.33)$$

$$V_r = 3.12 \times 10^3 (\rho Q_r)^{0.125}$$

where ρ is the air density (g/cm^3), Q_r the mixing ratio of raindrop (g/g), Q_v the mixing ratio of water vapor (g/g), Q_{vs} the saturation mixing ratio of water vapor (g/g), e_{vs} the saturation vapor pressure (hPa), C the ventilation coefficient, V_r the terminal velocity for raindrops (cm/s).

In order to apply this formula , the grid point into a cloud area are separated from its environmental area. When a grid point at the k-th level in the cloud area has condensation Δq_k (g/g) during one time step Δt , the flux of raindrops

at this level, $(\rho Q_r V_r)$ is calculated as follows

$$(\rho Q_r V_r)_k = (\rho Q_r V_r)_{k+1} + \frac{1}{\alpha_c} \frac{\Delta q_k}{\Delta t} \frac{\Delta p_k}{g} \quad (4.4.34)$$

where Δp_k denotes the thickness of the k-th level and the parameter α_c denotes a cloud amount. The raindrop flux is assumed to be confined in the cloud base. Below the cloud base, raindrops may evaporate and the flux will decrease. The air column below the cloud area may be wetter than the environmental field. Hence, It is assumed that the mixing ratios Q_v and Q_{vs} in eq. (4.4.33) are given by

$$Q_v - Q_{vs} = \beta_c (Q_v - Q_{vs})_{gr} \quad (4.4.35)$$

where subscript gr indicates the grid point value and the parameter β_c is equal to or less than unity. The flux below the cloud base is written as

$$(\rho Q_r V_r)_k = (\rho Q_r V_r)_{k+1} - P7_k \frac{\Delta p_k}{g} \quad (4.4.36)$$

Eqs. (4.4.33) - (4.4.36) yield the flux and evaporation of raindrops successively downward from the unstable top level. The temperature and mixing ratio change of the k-th level due to the evaporation are given by

$$\begin{aligned} \Delta T_k &= -\alpha_c L P7_k \Delta t \\ \Delta Q_k &= \alpha_c P7_k \Delta t \end{aligned} \quad (4.4.37)$$

The parameters α_c and β_c are set unity in RSM.

(f) Targeted moisture diffusion

In addition to ordinary 4th order horizontal diffusion (see 4.4.7), enhanced 2nd order diffusion is applied to moisture field targeting a strong upward motion. It can prevent a pseudo small low from developing over ocean by effectively suppressing excessive grid-scale updrafts and rainfalls.

(g) Parameterization of water loading

The water loading has a greater impact for rainfall forecast than the non-hydrostatic effect at the horizontal resolution of 20km (e.g. Kato and Saito, 1995). Then the effect of water loading is included the hydrostatic equation as follows:

$$\frac{\partial \phi}{\partial \eta} = -\frac{1}{\frac{p}{R_d T_v} + \rho_r} \frac{\partial p}{\partial \eta} \quad (4.4.38)$$

where ρ_r is the density of rain water, which is given by ρQ_r in equation (4.4.34).

(h) Radiation

The basic framework of the radiation scheme is described in 4.2. The long wave radiation is calculated hourly and modified by the changing the surface temperature at every time step. The short wave radiation is calculated hourly and modified by the changing the solar zenith angle at every time step.

The cloud amount at each level is obtained by an empirical relation between the cloud amount and the relative humidity (Ohno et al., 1984), while the cloud amount at the lowest 5 levels are set to zero. Maximum overlapping of the clouds is assumed in the vertical.

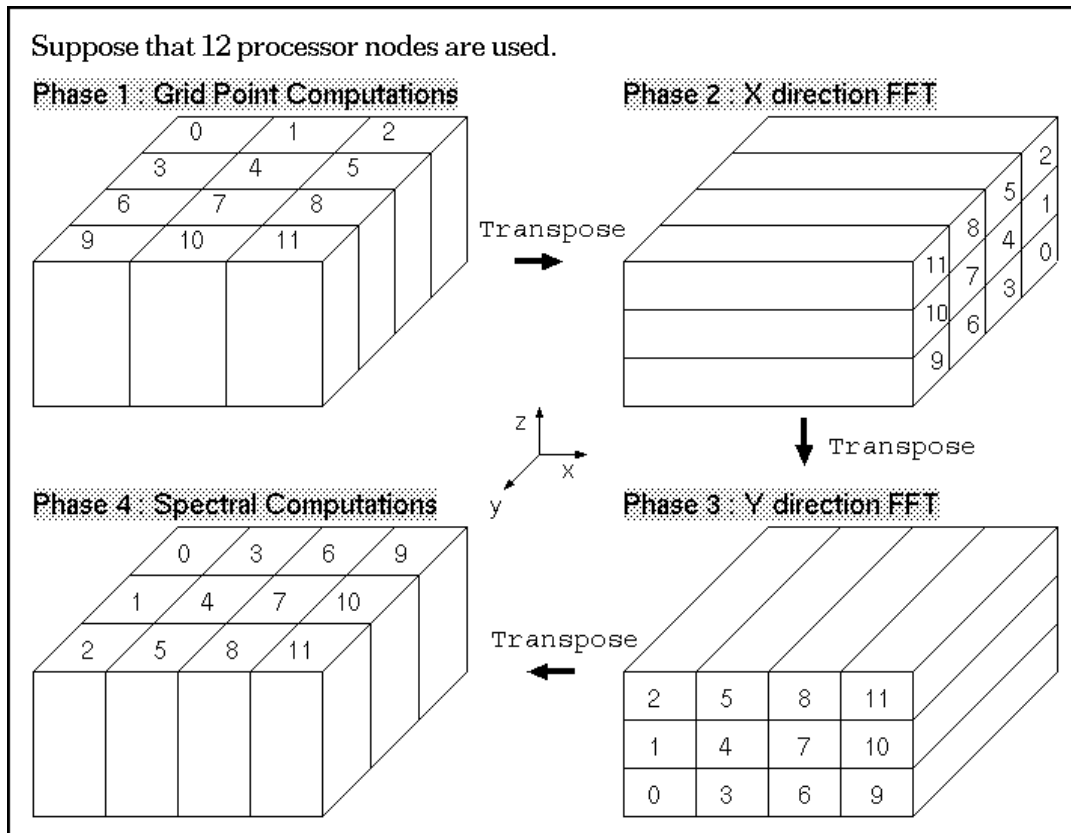


Fig. 4.4.2 Four computational phases involved in parallelized RSM

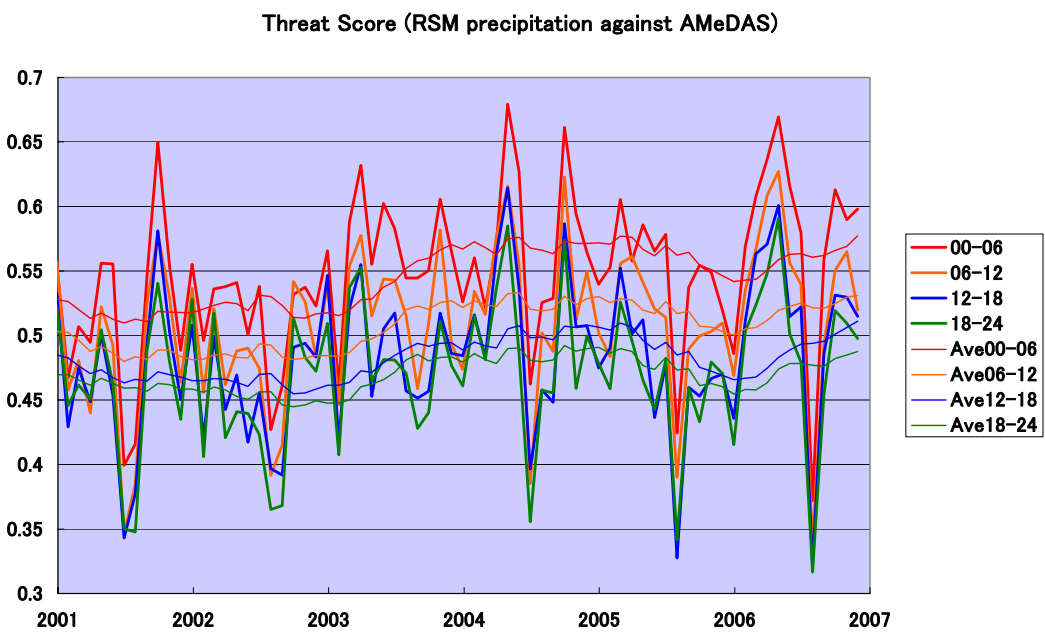


Fig. 4.4.3 The monthly mean threat scores of 6 hours precipitation by RSM with a threshold of 1mm per 6 hours.

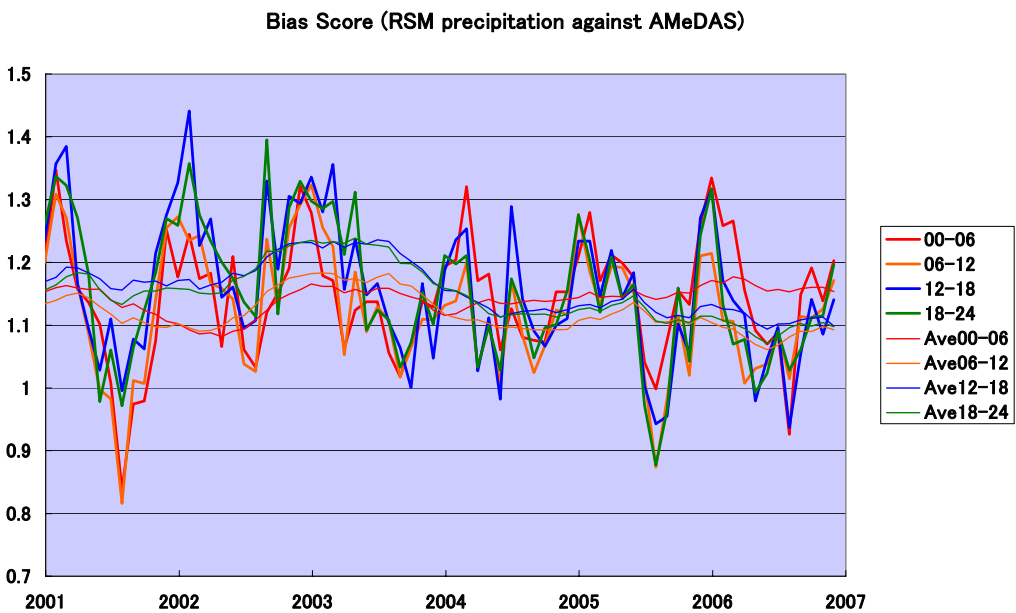


Fig 4.4.4 Same as Fig. 4.4.3 but bias scores.

(i) Gravity wave drag

The effect of the gravity waves induced by subgrid scale orography is included. The scheme is developed by Iwasaki et al. (1989) and described in 4.2. Though the original scheme consists of two parts, long wave and short wave scheme, only the short wave scheme is adopted.

4.4.9 Initialization

The nonlinear normal mode initialization for limited area model by Takano et al. (1989) is used to suppress the high frequency gravity wave noise. The normal modes of the model are calculated for the stratified atmosphere at rest with horizontally uniform temperature by assuming a constant map factor and constant Coriolis parameter. The horizontal structure functions of the normal modes are the same as the double Fourier function used in the spectral representation described in 4.4.4. The first five vertical modes of periods less than 6 hours are initialized, i.e., their time tendencies are set to zero. The initialization procedure is iterated four times using Machenhauer's method (Machenhauer, 1977). Physical processes are included in calculating the time tendencies of the normal models. The remaining vertical modes of the wave components are fixed during the iteration.

4.4.10 Parallelization

RSM is operated at the distributed memory machine since March 2001. Message Passing Interface(MPI) is adopted to parallelize the source code of RSM. Fig. 4.4.2 shows the four computational phases to calculate the orthogonal double Fourier series transform.

4.4.11 Performance of RSM

The prediction of precipitation is one of the most important target of RSM. Fig. 4.4.3 and Fig. 4.4.4 shows the monthly mean threat score and bias score of 6-hour precipitation predicted by RSM with a threshold at 1mm.

References

- Arakawa, A. and W.H. Schubert. 1974. Interaction of a cumulus cloud ensemble with the large-scale environment, Part I. *J.Atmos. Sci.*, **31** : 674–701.
- Arakawa, A. and V.R. Lamb, 1977: Computational design of the basic dynamical processes of the UCLA general circulation model. *Methods in Computational Physics*, **17**, Academic press, 174–265.
- Baba, A., 1986: An objective Analysis of Sea Surface Temperature. *JMA/NPD Technical Reports*, No. 5.
- Benwell, G.R.R. and F.H. Bushby, 1970: A case study of frontal behavior using a 10-level primitive equation model.

- Quart. J. R. Met. Soc.*, **96**, 287–296.
- Davies, H.C., 1976: A lateral boundary formulation for multi-level prediction models. *Quart. J. Roy. Met. Soc.*, **102**, 405–418.
- Gadd, A.J., and J.F. Keers, 1970: Surface exchanges of sensible and latent heat in a 10-level model atmosphere. *Qurt. J. Roy. Met. Soc.*, **96**, 297–308.
- Kato, T. and K. Saito, 1995: Hydrostatic and nonhydrostatic simulation of moist convection: The applicability of hydrostatic approximation to a high-resolution model. *J. Met. Soc. Japan*, **73**, 58–77.
- Kondo, J., 1975: Air-sea bulk transfer coefficients in diabatic conditions. *Bound. Layer Met.*, **9**, 91–112.
- Louis, J.F., M. Tiedtke and J.F. Geleyn, 1981: A short history of the operational PBL-parameterization at ECMWF, Workshop on Planetary Boundary Layer Parameterization 25-27 Nov. 1981, 59–79.
- Machenhauer, B., 1977: On the dynamics of gravity oscillations in a shallow water model with applications to normal mode initialization. *Beitr. Phys. Atmos.*, **50**, 253–271.
- Matthews, E., 1983: Global vegetation and land use: new high-resolution data bases for climate studies. *J. Clim. Appl. Met.* **22**, 474–487.
- Mellor, G.L. and T. Yamada, 1974: A hierarchy of turbulence closure models for planetary boundary layers. *J. Atmos. Sci.*, **31**, 1791–1806.
- NPD/JMA, 1986: *Outline of operational numerical weather prediction at Japan Meteorological Agency*.
- Ogura, Y. and T. Takahashi, 1971: Numerical simulation of the life cycle of a thunderstorm cell. *Mon. Wea. Rev.*, **99**, 895–911.
- Ohno, H. and M. Isa, 1984: A statistical relation between GMS-viewed cloud amount and relative humidity. *Tenki*, **31**, No.8, 493–495. (in Japanese)
- Segami, A. , K. Kurihara, H. Nakamura, M. Ueno, and I. Takano, 1989: Description of Japan Spectral model. *JMA/NPD Technical Reports*, No. 25.
- Segami, A., K. Kurihara, H. Nakamura, M. Ueno, I. Takano, and Y. Tatsumi, 1989: Operational Meso Scale Weather Prediction with Japan Spectral Model. *J. Met. Soc. Japan*, **67**, 907–924.
- Takano, I., H. Nakamura, and Y. Tatsumi, 1988: Nonlinear NMI for spectral limited area models. *JMA/NPD Technical Reports*, No. 26.
- Tatsumi, Y., 1986: A spectral limited-area model with time dependent boundary conditions and its application to a multi-level primitive equation model. *J. Met. Soc. Japan*, **64**, 637–663.
- Tatsumi, Y., 1987: A spectral limited-area model with time-dependent boundary conditions, Short and Medium-range Numerical Weather prediction, Met. Soc. of Japan, 473–483.
- Tokioka, T., K. Yamazaki, A. Kitoh, and T.Ose, 1988: The equatorial 30-60 day oscillation and Arakawa-Schubert cumulus parameterization. *J. Met. Soc. Japan*, **66**, 883–900.
- Troen, I.B and L. Mahrt, 1986: A Simple Model of the Atmospheric Boundary Layer; Sensitivity to Surface Evaporation. *Boundary-Layer Met.*, **37**, 129–148.